Dynamics and regulation at the tip : a high resolution view on microtubele assembly

Munteanu, L.

CHAPTER

5 Regulation of microtubule dynamics by the autonomous microtubule-end tracker Mal3

+TIPs are intriguing proteins that have the special ability to localize at the microtubule growing ends. This advantageous position enables +TIPs to directly regulate the microtubule dynamics. EB1 protein family members were shown to affect microtubule dynamics and organization in vivo, but it is still unclear if the EB proteins exert an effect on microtubule dynamics on their own. In this chapter we investigated the effect of such a +TIP from the EB1 protein family, namely the fission yeast homologe, Mal3. Our results show that, in vitro, Mal3 is an autonomous end tracker of growing microtubule ends. Here we investigate the effect of Mal3 on the microtubule plus-end growth dynamics using light microscopy, fluorescence microscopy and our high-resolution technique based on optical tweezers. Using time-lapse DIC and fluorescence imaging of individual microtubules we find that Mal3 binds differentially to the lattice and at the tip of a growing microtubule and the presence of Mal3 affects all the parameters of microtubule dynamic instability. Mal3 binds efficiently at the microtubule tip where it enhances tubulin dimer net addition and the chance for a microtubule to switch from a growing to a shrinking phase. Microtubules in the presence of Mal3 grew up to 3-fold faster and had up to 4-fold enhanced catastrophe rate. Using our high-resolution technique we could identify incomplete microtubules, most probably resembling the end-structures at the growing tip, that were formed in the presence of Mal3. In the fluorescent measurements we identified longer Mal3-decorated end-structures with increasing Mal3 concentrations. At the microtubule lattice Mal3 binds less potently than at the tip. With Mal3 present at the lattice, the microtubules disassembled slower and rescues were highly promoted. Our results suggest that Mal3 has a complex influence on microtubule dynamics, both stabilizing and destabilizing and that Mal3 induced effects are correlated with a differential binding of Mal3 at the tip and on the lattice of a growing microtubule.

5.1 Introduction

Mal3 is the fission yeast homolog of end-binding 1 (EB1) protein. EB1 family members are highly conserved regulators of microtubule dynamics belonging to the core part of the interaction network formed by the microtubule plus-end binding proteins [14]. Human EB1 added to *Xenopus* egg extracts promotes microtubule growth by increasing the rescue rate and decreasing the catastrophe rate [110, 185]. The fission yeast homologue Mal3 was also shown to promote initiation of microtubule growth and to inhibit catastrophes. Cells that are lacking Mal3 have shortened microtubules with premature catastrophes [108, 109].

In order to dissect the influence of the end-binding proteins on the microtubule dynamics we need an *in vitro* assay, in which the *in vivo* localization of the proteins on dynamic microtubules is preserved and individual microtubules can be monitored in the presence of one protein or a system of end-binding proteins. The growth promoting effect of EB1 and Mal3 on microtubules was previously suggested from bulk turbidity assays [25, 112] that reflect the influence of the proteins on the total polymer formed [170] and do not give information about the influence on the dynamics of individual microtubules. Experiments were also performed on individual microtubules in egg extracts [110] and in cells [109, 113, 114]. In these experiments, the environment in which the microtubules assemble contains a cocktail of proteins and therefore the sole influence of EB1 or Mal3 on microtubule dynamics cannot be inferred.

As described in chapter 4, Mal3 is a microtubule-end tracker *in vitro* with similar end-tracking behavior as *in vivo*. Mal3 is able to accumulate both at the plus and minus ends of growing microtubules and not on the ends of shrinking or stable microtubules. Strikingly, this behavior does not depend on the presence of other end-tracking proteins. Here we investigate the influence of Mal3 on the dynamics of individual microtubules and the molecular mechanism of interaction with the microtubule end. Dynamic microtubules were nucleated from centrosomes in order to selectively probe the plus end dynamics of microtubules.

5.2 Results

5.2.1 Mal3 enhances the dynamic instability of microtubules *in vitro*.

In the presence of Mal3 we observed a change in all dynamic instability parameters: growth speed, shrinkage speed, catastrophe rate and rescue rate.

For Mal3 concentrations ranging from 20 nM to 200 nM, the growth speed was enhanced in a concentration dependent manner: the more Mal3 present, the faster the microtubules grew (figure 5.1 b). Mal3 sped up the microtubule growth to a maximum of 3-fold achieved at a ratio of Mal3 : tubulin of approximatively 1 : 70. For Mal3 concentrations higher than 200 nM, the average growth speed remained constant at the 3-fold enhanced level (figure 5.1 b). The effect of Mal3 on shrinkage speed was less strong.

The presence of the end binding protein slowed down depolymerizing microtubules. For concentrations less than 200 nM Mal3, the effect on the shrinkage speed was concentration dependent (figure 5.1 c). We measured a constant 1.5-fold reduction in the shrinkage speed in the presence of more than 200 nM Mal3.

Microtubules grow and shrink with intrinsically variable speeds [186]. This variability is reflected by the standard deviation, sd, over the speeds of individual growth and shrinkage events. We typically measured sd values of 20% to 30% of the average microtubule growth and shrinkage speeds. We did not observe an influence of Mal3 on the sd, indicating that Mal3 had no effect on the intrinsic variability of microtubule growth and shrinkage.

The most striking effect we measured in the presence of Mal3 was the increased catastrophe rate (figure 5.1 d), as opposed to the *in vivo* case where the absence of Mal3 results in more dynamic microtubules [108, 109]. We observed that the catastrophe rate *in vitro* was increasing with the concentration of Mal3, to a maximum of 0.20 ± 0.02 min^{-1}, which is 4-fold higher than the catastrophe rate we measured in control samples (no Mal3: 0.050 ± 0.006 min^{-1}). This maximum was reached around 100 nM Mal3 corresponding to a Mal3 : tubulin ratio of 1 : 150. For Mal3 concentrations higher than 100 nM, the catastrophe rate was slowly decreasing to 0.14 ± 0.02 min^{-1}, which was still 3-fold higher than the control level.

Mal3 had a strong concentration dependent effect on the rescue frequency as well (figure 5.1 e). We measured a more than 10-fold increase in the rescue rate in the range from 100 nM to 2.5 μM Mal3. The increase was approximately linear with the Mal3 concentration and the rescue rate did not saturate in the range of concentrations we investigated. For Mal3 concentrations below 200 nM we were not able to calculate a reliable rescue frequency due to the low number of events observed and only an upper bound could be estimated (data analysis described in section 5.5.1).

The addition of new tubulin subunits, reflected in the growth speed, as well as the initiation of a shrinkage phase, reflected in the catastrophe rate, happens at the microtubule tip. We saw a similar influence of Mal3 on the two processes: at low Mal3 concentrations, the Mal3-induced enhancement was proportional with the amount of Mal3 present in solution and above a certain concentration, the effect saturated. The rapid disassembly of tubulin, evaluated as shrinkage speed, and the chance of switching from a shrinkage to a growing phase, the rescue rate, depend mostly on the microtubule lattice properties. We observed a different behavior for the rescue rate as compared with the catastrophe rate: we measured a continuously increasing rescue rate proportional to the Mal3 concentration and no saturation of this effect. Shrinkage speed had yet similar behavior as the growth speed and catastrophe rate. These differences between the effects of Mal3 on the dynamic instability parameters might reflect a differential interaction of Mal3 with the tip and with the microtubule lattice. Therefore we next investigated the localization of Mal3 on the dynamic microtubules at similar conditions used to determine the dynamic instability parameters.

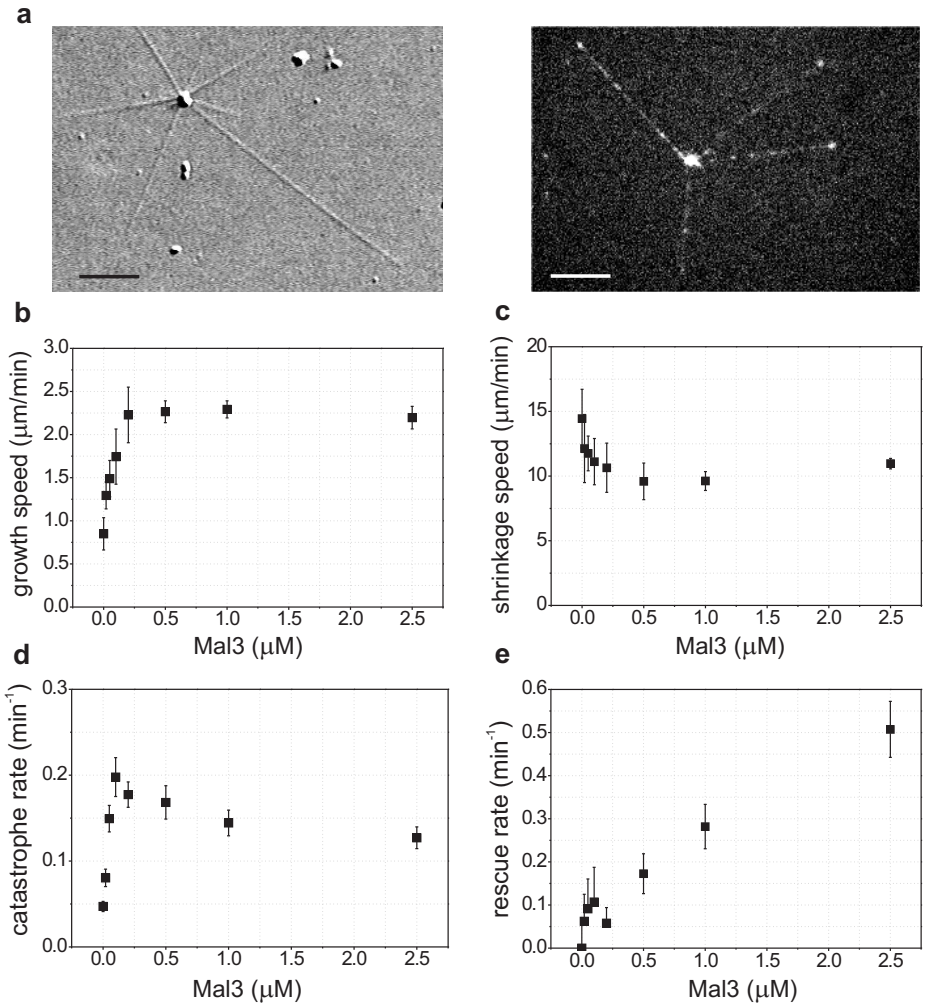

Figure 5.1: Dynamic instability parameters. **(a)** A video-enhanced DIC micrograph of centrosome nucleated microtubules (left) and a confocal image showing the Mal3-Alexa 488 (100 nM) tracking the microtubule growing ends (right). Scale bars are 5 μm. **(b)** Growth speeds, **(c)** shrinkage speeds, **(d)** catastrophe rates and **(e)** rescue rates of microtubules in the presence of different concentrations of Mal3. Microtubules were assembled from 15 μM tubulin and with 50 mM KCl present in solution, at 25 ^{o}C. For each data point we cumulated data from 3 - 6 independent experiments. Data are presented as (mean ± sd) (data analysis described in section 5.5.1).

5.2.2 Mal3 interacts differentially with the tip and with the lattice of growing microtubules.

We showed in chapter 4 that Mal3 tracks the ends of growing microtubules by an end recognition mechanism, i.e. having an enhanced binding at the growing end structure as compared with the lattice [124]. In order to investigate if there is a correlation between the observed changes in the microtubule dynamics and the differential binding of Mal3 on the microtubules, we used confocal microscopy to image Alexa 488 labelled Mal3 on dynamic microtubules.

For each Mal3 concentration we analyzed profiles from 3 - 4 independent experiments and in each experiment 10 - 70 microtubules were analyzed. We first evaluated the average Mal3-Alexa 488 background intensity in each experiment in order to test the quality of our method employed for the image processing and the profile analysis (section 5.5.2). We expect a linear dependency between the Mal3 concentration and the average Mal3-Alexa 488 background intensity measured in each experiment. Figure 5.2 b shows indeed a linear dependency of the average background intensity, $I_{\text{background}}$, on the Mal3 concentration. The spread in the background intensity between the samples prepared at the same Mal3 concentration was significant, especially at low Mal3 concentrations (inset in figure 5.2 b). This spread is due to the errors in the protein concentrations resulting from the sample preparation. In order to exclude the experimental errors, we chose to present quantities evaluated from the profile analysis as a function of the background intensity.

The microtubule profiles of Mal3-Alexa 488 showed a clear difference between the signal at the tip and on the microtubule lattice (figure 5.2 a) for the whole range of Mal3 concentrations investigated. From the microtubule profiles we evaluated three quantities: the relative amount, as compared with a control sample, of Mal3 bound on the microtubule lattice, I_{lattice}, the amount interacting with the microtubule growing end, I_{tip}, and the typical length of the tip signal, σ_{tip} (see section 5.5.2).

The average signal on the lattice was increasing proportionally with the amount of Mal3 present in solution (a linear fit seems to be a good approximation to the data, figure 5.2 d), indicating a simple first-order interaction of the protein with the microtubule lattice. Mal3 was shown to bind preferentially at the seam [25], but we do not exclude binding elsewhere on the lattice. The lattice binding sites for Mal3 did not saturate in the range of Mal3 concentrations investigated here. This linear-increase behavior is very similar with the one observed for the rescue rate in the presence of Mal3 (figure 5.1 e). The similarity of the two results indicates that the Mal3 bound on the microtubule lattice affects rescue rates. One of the possible underlying mechanisms, recently revealed by cryo electron-microscopy [25], is the increased stability of the microtubule lattice, primarily due to the microtubule seam stabilization by Mal3.

At the microtubule tip, remarkably, the average signal showed elevated intensity even at very low Mal3 concentrations demonstrating a potent binding of Mal3 at the growing end. This elevated efficiency of binding could be due to a low dissociation con-

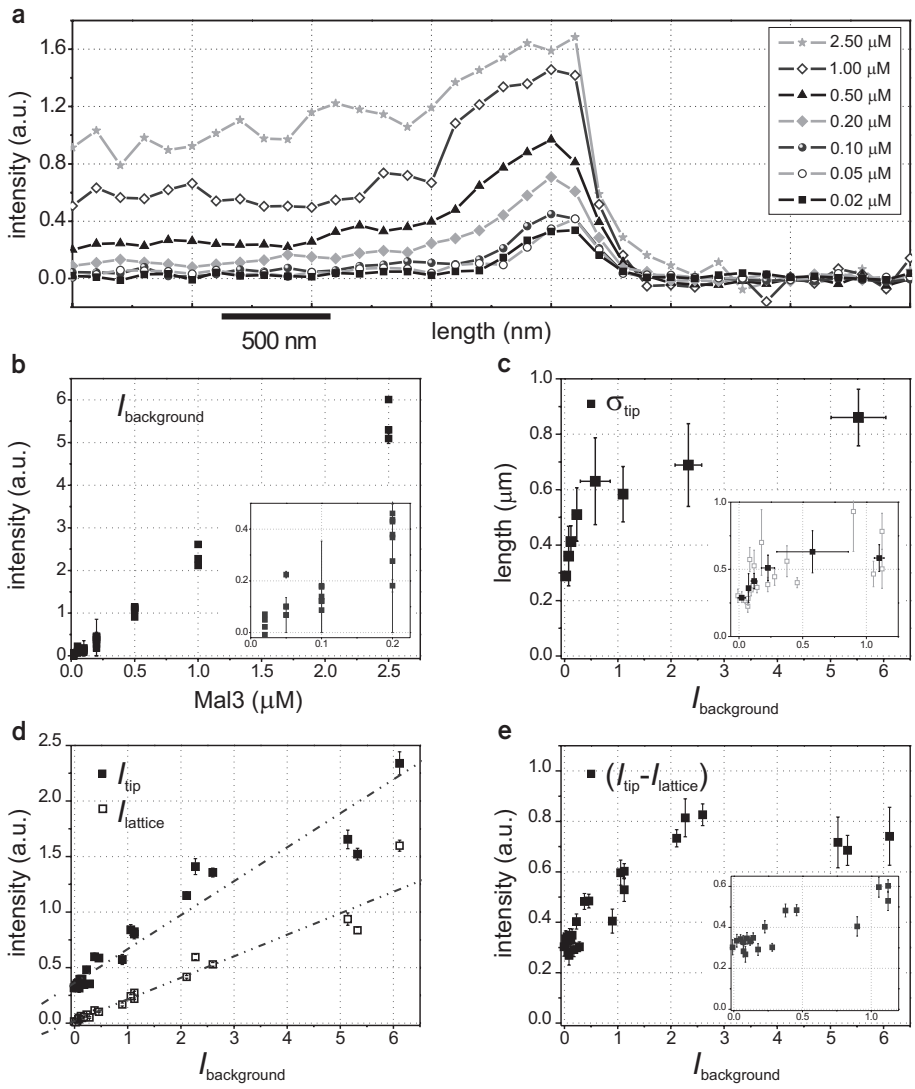

Figure 5.2: Mal3-Alexa 488 binds differentially on growing microtubules. **(a)** Mal3 intensity profiles along microtubules measured at the indicated concentrations of Mal3. Each profile is the average of about 10 - 70 microtubules from one experiment. **(b)** The normalized background intensity, $I_{\text{background}}$, as a function of the Mal3 concentration follows a linear relationship, as expected. **(c)** The spatial extent of the Mal3 signal at the microtubule tip, σ_{tip} as a function of the background intensity. The data (open symbols in the inset) were binned over 3 data points. The x-errors represent s.d. and the y-errors are s.e.m. **(d)** Normalized intensity of Mal3 present at the tip, I_{tip}, (solid symbols) and on the microtubule lattice, I_{lattice}, (open symbols) as a function of the background intensity. Dotted lines are linear fits to the data. The intensity I_{tip} was evaluated over the tip region, σ_{tip}. The difference, $(I_{\text{tip}} - I_{\text{lattice}})$, is shown in **(e)**. The normalized intensities presented in **(d)** and **(e)** represent values per image pixel (110×110 nm^2) and are proportional with the amount of Mal3 (see section 5.5.2). Data was collected from 24 independent experiments. Insets: zoom in the initial part of the data. Error bars represent s.e.m. For the difference signal, the errors were calculated by error propagation.

stant ($K_D = k_{off}/k_{on}$) of Mal3 at the tip compared with the lattice and/or due to a higher number of available binding sites. The sharp transition of the tip signal from zero (no Mal3 present in solution) to the condition with Mal3 present, followed by an almost linear increase in the tip signal (figure 5.2 d), indicate different interaction kinetics of the protein at the growing end as compared to the interaction with the microtubule lattice. When we plot the difference signal between the tip and the lattice (figure 5.2 e) we noticed a similar saturation behavior of the signal as for the microtubule growth speed and the catastrophe rate (figure 5.1 b and d). This observation implies that, at the tip, there are lattice-like binding sites that do not saturate in the regime of concentrations investigated and tip-specific binding sites that saturate, similarly with the growth speed and catastrophe rate. This correlation suggests that Mal3 present at the tip induces structural and/or biochemical changes at the tip that affect both the tubulin incorporation rate and the chance of switching to a shrinking phase.

We also measured an increase in the spatial extent of the tip signal with the Mal3 concentration (figure 5.2 c). The region with higher Mal3 concentration at the microtubule tip was increased more than 4-fold in the presence of Mal3 to a length of approximately 800 nm. At low concentrations of Mal3 we measured a spatial extent of the Mal3 signal of 250 nm, but the measurement is probably limited by the optical resolution. As shown in chapter 4 and [124], Mal3 most probably recognized an end-structure at the growing microtubule tip. Our result suggests that in the presence of Mal3 microtubules have longer end-structures. To further investigate the influence of Mal3 on these tip-specific structures we followed microtubule assembly and disassembly with our optical tweezers based technique that provides near molecular resolution.

5.2.3 Mal3 promotes formation of microtubule end-structures.

When Mal3 was present in high concentration (1 μM and higher), we sometimes observed curved, elongated structures at the end of growing microtubules (figure 5.3). These structures could be malformed tubes or some specific end structure different than a closed tube. The fact that the curved structure can be straightened while the microtubule is growing suggests that there is no defect in the tube growth, but rather an extended end-structure before closing into a tube. These observations together with the fluorescent measurements on Mal3 spatial extent at the tip suggest that Mal3 promotes formation of elongated microtubule end-structures. In order to gain more information about the changes induced by Mal3 at the microtubule tip we measured microtubule growth at high-resolution using optical tweezers (method described in chapter 2). Our preliminary experiments and observations are presented below.

Figure 5.4 a shows microtubule growth traces in the absence (upper panel) and in the presence of 200 nM Mal3 (lower panel) measured with optical tweezers. In these experiments, microtubules grew under force (indicated on the right axis), which is known to affect their dynamics [70, 76, 77]. In both experiments shown in figure 5.4 a the average and the maximum force experienced by the growing microtubules were similar.

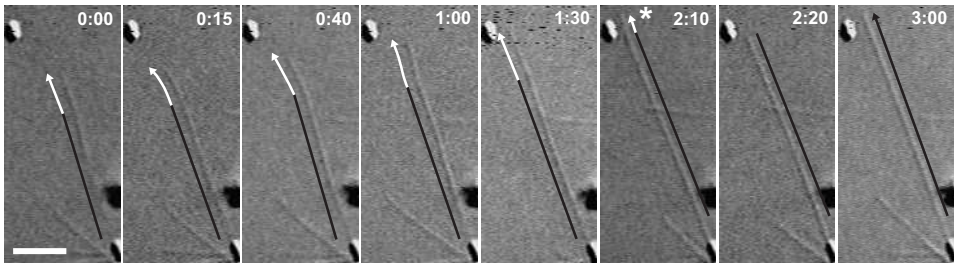

Figure 5.3: Microtubule end-structure in the presence of Mal3. Time sequence of DIC images of a growing microtubule in the presence of 1 μM Mal3. Schematic guiding lines (shifted with respect to the image) of the dynamic microtubule are drawn. An arrowed line indicates growth. A curved structure, 2 - 3 μm in length, (white part of the line) is elongating at the microtubule tip and straightens while the microtubule is growing (the black part of the line represents the straight microtubule). The end-structure had a catastrophe (asterisk in frame 2:10) and depolymerized until the straight part of the microtubule. The time elapsed from the first image is indicated in min : sec. Scale bar is 3 μm.

Zooming in on the high-resolution traces, we noticed variabilities in speeds during one continuous event both for the growth and for the shrinkage phases (figure 5.4 b). For the depolymerization events we could clearly identify two types of processes: slow and fast depolymerization (empty and solid arrow heads, respectively, in figure 5.4 b). The microtubule depolymerization events often started with a slow phase followed by a fast shrinkage. Sometimes multiple slow and fast length reductions were identified during a depolymerization event. We also observed shrinkage events that could be entirely described by slow depolymerization, mostly in the Mal3 samples (figure 5.4 b).

In order to quantify the effect of Mal3 on microtubule assembly and disassembly, we evaluated growth and shrinkage speeds of short data stretches where the growth and, respectively, the shrinkage speed was approximately constant (data analysis described in section 5.5.3). For the two conditions investigated (absence and presence of Mal3), we analyzed the growth and the shrinkage events of microtubules from two independent experiments (part of the two data sets are shown in figure 5.4 a). The distributions of speeds are shown in figure 5.5. In the optical tweezers experiments, the microtubule average length was much shorter (100-400 nm) as compared to the average length in the absence of force, in the DIC experiments (couple of micrometer). Therefore, our data from the high-resolution experiments refer to growth and shrinkage speeds on a smaller length and time scale. In the time scale there is typically a factor 10 difference between the two methods.

For the growth events we evaluated growth speeds only on stretches that displayed predominantly microtubule length increase and we excluded the more extensive pauses and length reductions during growth. Therefore the mean values are overestimated and the comparison between the effect of Mal3 on the growth speed measured with the two methods, optical tweezers and DIC, is only qualitative. In the absence of Mal3

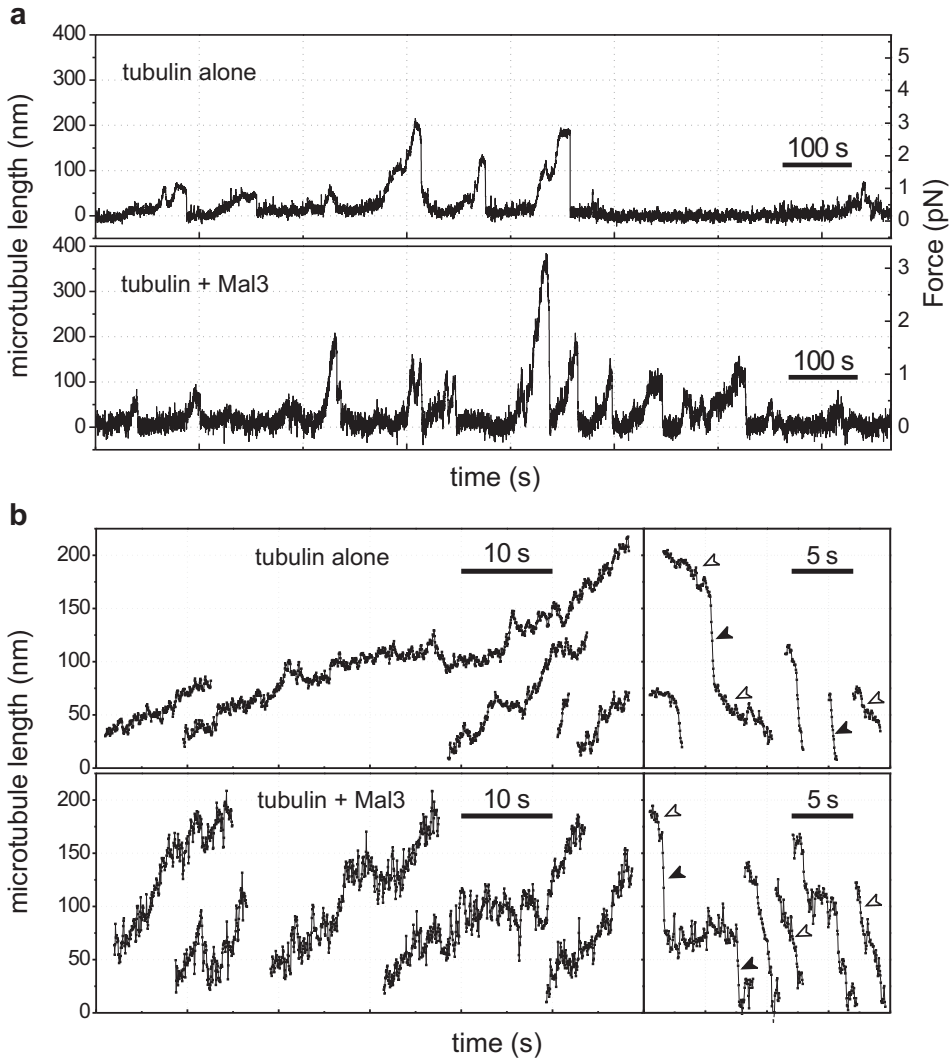

Figure 5.4: Microtubule assembly measured with optical tweezers. **(a)** Growth and shrinking events of individual microtubules in the absence (top panel) and in the presence of 200 nM Mal3 (lower panel). The microtubules grow and shrink in the presence of an opposing force (indicated on the right axis). **(b)** Selected growth and shrinkage events shown at higher magnification. Empty arrowheads indicate slow depolymerization phases and solid arrowheads indicate fast length decreases.

we measured reduced growth speeds with a weighted average of 0.48 ± 0.08 μm min^{-1} (mean ± s.e.m.; n = 18) as compared with the average growth speed measured on freely growing microtubules in the DIC experiment, 0.88 ± 0.03 μm min^{-1} (n = 99) (figure 5.5 a, top panel). This effect was expected due to the fact that microtubules in the optical

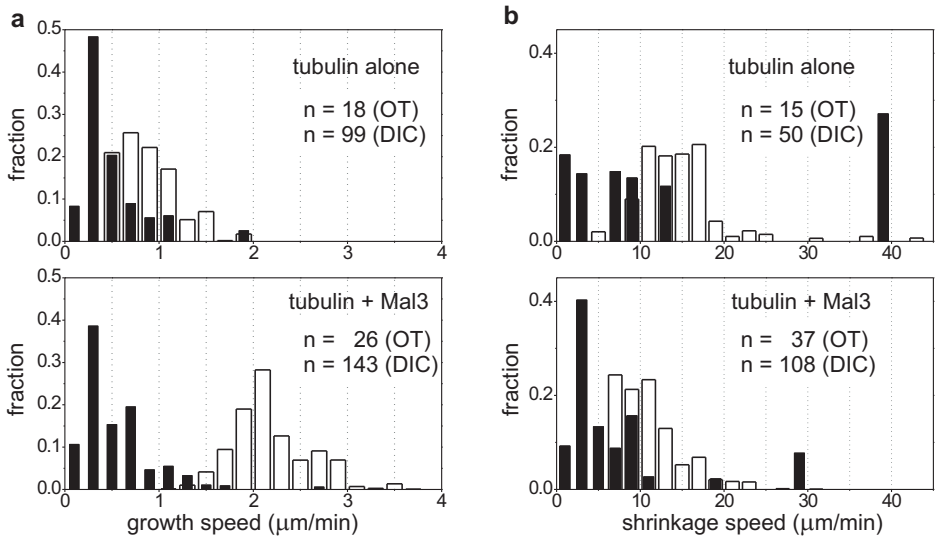

Figure 5.5: Quantifying growth and shrinkage speeds. Weighted distributions of **(a)** growth speeds and **(b)** shrinkage speeds for microtubules grown in the absence (top panels) and in the presence of 200 nM Mal3 (lower panels). The empty-bar distributions were evaluated from the DIC experiments with microtubules growing freely from centrosomes. The black solid-bar distributions were evaluated from the high-resolution measurement with optical tweezers (OT). The contribution of each speed in the distributions was weighted with the time extent of the corresponding event for the DIC data, growth and shrinkage events, and for the OT data, only growth events. Each shrinking event measured with the OT was weighted with the length reduction during the event. The total number of data stretches (n) used to compute the distributions are indicated.

tweezers experiment were growing against a force, which reduces the growth speed [70,76,77]. In the presence of Mal3 the average growth speed was reduced more strongly from 2.18 ± 0.03 μm min^{-1} without force (n = 143) to 0.53 ± 0.07 μm min^{-1} under force (n = 26) (figure 5.5 a, lower panel). This effect could be interpreted in two ways: i) force has a different effect on microtubule growth when Mal3 is present at the end, consistent with an altered end-structure in the presence of Mal3 or ii) the presence of an opposing force impedes Mal3 to exert its effect at the microtubule tip. More experiments are necessary to elucidate the underlying mechanism.

Shrinkage speed distributions evaluated from the high-resolution traces displayed an interesting behavior as compared to the DIC data analyzed at low-resolution. We measured a relatively high number of data stretches that displayed a much lower shrinking speed than the average speed measured in the DIC experiment, both for the tubulin alone and in the presence of 200 nM Mal3. These slow events appear in the weighted distribution as peaks in the speed range below 5 μm min^{-1} (figure 5.5 b). The slow events were typically present at the onset of the depolymerization phases, spanning few tens of nanometers and a couple of seconds. In DIC we would not be able to mea-

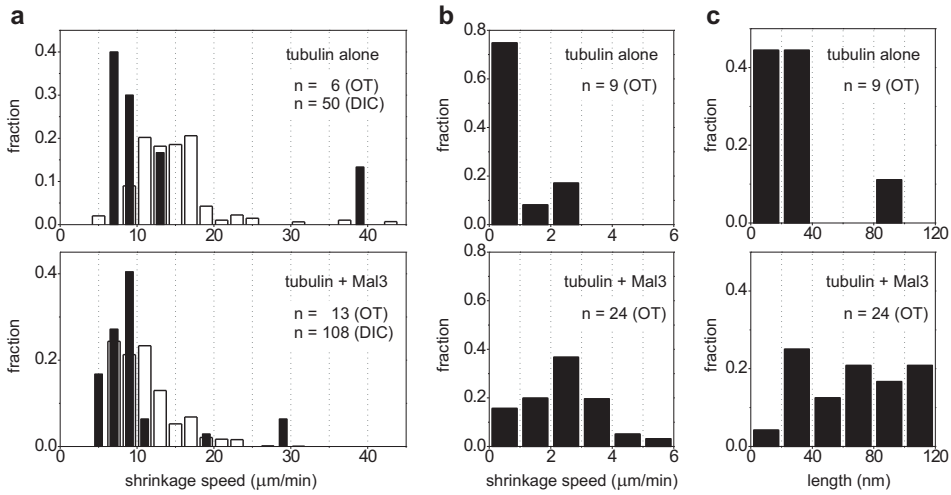

Figure 5.6: Quantifying the slow and the fast shrinkage events. Weighted distributions of **(a)** fast and **(b)** slow shrinkage speeds for microtubules grown in the absence (top panels) and in the presence of 200 nM Mal3 (lower panels). The empty-bar distributions were evaluated from the DIC experiments with microtubules growing freely from centrosomes. The black solid-bar distributions were evaluated from the high-resolution measurement with optical tweezers (OT). The contribution of each speed in the distributions was weighted with the time extent of the corresponding event. **(c)** Length distributions of the slow disassembly stretches in the presence and absence of Mal3. The slow events are the same as used in **(b)**.

sure such events, given the typical resolution of microscopy. Therefore, the most probable explanation for the lack of peaks below 5 $\mu m\,min^{-1}$ in the DIC data is the limited resolution of the DIC method.

Due to the fact that almost all shrinkage events started with a slow length-decrease followed by fast depolymerization, we think that the slow length-decrease represents the event that triggers microtubule fast depolymerization. As further discussed in chapter 6 this event could be the disassembly of the end-structure or loss of lateral contacts between the protofilaments at the microtubule tip. Following this idea, the shrinkage events that are completely described by slow length-decrease could represent disassembly of incomplete microtubules that only have an end-structure, which did not yet close into a tube to form a regular microtubule lattice.

To further investigate the possible influence of Mal3 on these slow depolymerization phases we evaluated weighted speed distributions separately for the fast and the slow events (figure 5.6). Slow speeds were selected as speeds in the range below the minimum shrinkage speed measured in the DIC experiment ($< 5.5\ \mu m\,min^{-1}$). The fast speeds represent the speeds higher than this threshold ($> 5.5\ \mu m\,min^{-1}$). For the fast length reductions we measured similar average speeds at high- and low-resolution (figure 5.6 a). Mal3 slowed down depolymerizing microtubules in both experiments: from

13 ± 5 μm min^{-1} (n = 6) for tubulin alone to 10 ± 2 μm min^{-1} (n = 13) in the presence of Mal3 measured with optical tweezers, similar to the decrease from 14 ± 1 μm min^{-1} (n = 50) to 11 ± 0.4 μm min^{-1} (n = 108) in the DIC experiment (weighted average speeds are presented as mean ± s.e.m.). This similarity suggests that the fast length decreases measured with optical tweezers are underlined by regular microtubule depolymerization.

In contrast, the slow shrinkage events most probably reflect depolymerization of a different microtubule structure, e.g. an open tube or a sheet-like structures, or a conformational change at the tip (see also chapter 6). The speed and length distributions for the slow length-decreases are shown in figure 5.6 b and c. From the total microtubule length in the shrinkage phases approximately 60% was lost through slow disassembly in the presence of Mal3, while for tubulin alone only 33% of the total length was covered by the slow stretches. In the presence of Mal3 slow shrinkage occurred at an average speed of 2.4 ± 0.3 μm min^{-1} (n = 24) and the slow events had an average length of 67 ± 6 nm. In the absence of the protein the slow phases of depolymerization had an average speed of 1.0 ± 0.3 μm min^{-1} (n = 9) and an average length of 28 ± 7 nm. Average speeds and lengths are presented as mean ± s.e.m. The differences in speed and average length might reflect different events at the microtubule end: one prior to fast shrinkage, both in the absence and in the presence of Mal3, and one representing depolymerization of incomplete microtubules, observed mostly in the Mal3 sample. Only in the presence of Mal3 we frequently observe complete slow depolymerization events, pointing to fact that Mal3 promotes formation of end-structures. Further experiments are necessary to elucidate the nature of slow depolymerization and the influence of Mal3 on the end-structure (see also discussion in chapter 6).

5.3 Discussion

We found that Mal3 influences microtubule dynamics in various ways. Mal3 bound potently to the tip of growing microtubules. The protein presence at the tip enhanced the addition of tubulin dimers and increased the chance of catastrophes. On the other hand Mal3 had a stabilizing effect on the pre-existing protofilaments that form the lattice as we measured reduced shrinkage speeds and increased microtubule rescue rates.

The enhancement of tubulin net incorporation at the microtubule end in the presence of Mal3 could be explained by two scenarios: i) Mal3 binds to tubulin in solution and the formed complexes have higher affinity for the microtubule tip or ii) Mal3 binds at the microtubule growing end and induces changes that in turn facilitates the addition of new tubulin subunits. As described in chapter 4, the average time Mal3 decorated the microtubule-ends was much higher than the dwell time of individual Mal3 molecules (the time one molecule stayed bound) at the microtubule tip. This indicates that Mal3 recognizes the growing end-structure where it turns over rapidly. Also, gel filtration experiments revealed a weak interaction between tubulin and Mal3 in solution [124].

Taken together, these observations support the second scenario, in which Mal3 binds at the tip and changes the microtubule end-structure, most probably both biochemically and structurally. The tubulin dimers will have higher affinity for this Mal3-decorated end-structure. However, some contribution of the first scenario cannot be excluded, but due to the weak interaction between tubulin and Mal3 in solution, only a small amount of tubulin will be incorporated through enhanced co-polymerization of Mal3-tubulin complexes. The fact that we saw a saturation in the Mal3-induced enhancement of the growth speed indicates that the binding sites for Mal3 at the microtubule tip are limited. This idea is also supported by the observed saturation of the fluorescent Mal3 signal at the microtubule end (the tip signal above the lattice one) in the high range of concentration investigated. We observed a concentration lag between the saturation regime for the amount of Mal3 interacting at the microtubule tip and the saturation regime of the microtubule growth speed. This could mean that the microtubule end-structure recognized by Mal3 includes a higher number of Mal3 binding-sites than the ones where Mal3 affects tubulin incorporation.

In the presence of Mal3, we measured longer end-structures at the microtubule tip by monitoring the spatial extent of the region decorated with fluorescent protein at the microtubule tip. Longer end-structures in the presence of Mal3 could be explained by the increased microtubule growth speed, as previous electron microscopy experiments showed that faster growing microtubules display longer sheet-like structures at the growing end [34]. Indeed, the length enhancement of the Mal3 decorated end-structure correlated with the growth speed enhancement in the presence of Mal3. This effect was measured also when tubulin concentration was varied resulting in faster growing microtubules decorated by longer Mal3 comets (chapter 4).

According to previous data measured on dynamic microtubules [56,57], an increase in the growth speed correlates with a lower catastrophe rate. We measured an opposite effect in the presence of Mal3. The increased catastrophe rate induced by Mal3 correlated with the increase of the growth speed, showing that the protein bound at the microtubule end is not only enhancing the net rate of tubulin subunit incorporation, but also the chance of having a catastrophe. Our high-resolution data on disassembling microtubules revealed that Mal3 promotes formation of end-structures that depolymerize before closing into a regular microtubule. This effect could contribute to the increased switching from a growing to a shrinking phase. Previous work done *in vivo* suggested that removal of Mal3 from microtubule tips may be a prerequisite for a catastrophe to occur [109]. Our data suggest that Mal3 is most probably "removed" together with the tubulin by disassembly of the end-structure.

After a maximal Mal3-induced enhancement of the catastrophe rate we observed a slow decrease in the rate with Mal3 concentration. The catastrophe rate remained though elevated as compared with the tubulin control. These observations indicate that Mal3 present at the tip had both destabilizing and stabilizing effects. *In vivo*, the ratio Mal3:tubulin is in the order of 1:200 as roughly estimated from a bulk experiment

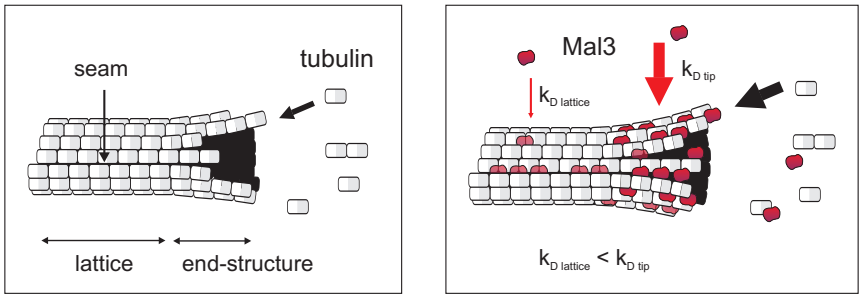

Figure 5.7: Schematic drawing of a growing microtubule end in the absence (left) and in the presence of Mal3 (right). Mal3 interacts differentially at the microtubule end and on the lattice.

[25]. This ratio, in our experiments, correlates with a region of Mal3 concentration after the maximum enhancement of the catastrophe rate induced by Mal3.

The dual effect of Mal3 observed on the catastrophe rate is underlined by the interaction of Mal3 and tubulin at the microtubule tip. As the end-structure present at the tip is continuously growing and changing into a tube, the interaction of Mal3 at the tip could be most probably described by a combination of end-specific interactions and lattice-like interactions. The destabilizing effect of Mal3, probably due to the end-specific interactions, seemed to be predominant. The end-structure that resemble the lattice could be responsible for the second stabilizing effect, though less potent.

We did not detect an accumulation of Mal3 at the tip of shrinking microtubules. Therefore the observed increase in the rescue rate and the decrease in the shrinkage speed might be correlated with a change in the lattice properties. The rescue rate increase was proportional with the amount of Mal3 on the lattice and in solution, whereas the shrinkage speeds after an initial decrease remained constant when we increased Mal3 concentration. This could suggest that Mal3 has a dual effect also at the lattice. Previous work showed that Mal3 binds preferentially to the seam of microtubules and increases the lattice stability [25]. This increased stability could be dependent on the amount of Mal3 bound to the seam. Shrinkage speed might be mainly influenced by the seam stability. Assuming this correlation between the amount of Mal3 present at the seam and the shrinkage speed (the more Mal3 at the seam, the more stable lattice and slower shrinking microtubules), we expect a saturation in the down-regulation by Mal3 of the shrinkage speed when the seam binding sites are saturated with Mal3. Our data supports this idea. However, the amount of Mal3 bound on the lattice did not saturate in the range of concentrations investigated. This could be an indication that Mal3 binds on the whole lattice, not only at the seam. The rescue rate enhancement correlates with the amount of Mal3 interacting with the lattice, suggesting that the protein on the lattice has an influence on the recovery of microtubules during shrinking events. Although we did not detect fluorescent signal of Mal3-Alexa 488 at the tip of shrinking microtubules, we cannot exclude an end-effect of Mal3 that enhances rescue rates. Fur-

ther experiments are needed to elucidate the extent of Mal3-binding sites at the lattice and whether Mal3 has an interaction with the shrinking microtubule ends.

In conclusion, Mal3 affects differentially the tip and the microtubule lattice (figure 5.7). At the microtubule end, Mal3 binds efficiently, where it enhances the tubulin incorporation and promotes catastrophes. At the lattice, Mal3 binds and stabilizes lattice-specific structures that are also present, to some extent, within the microtubule end-structure. As a result Mal3 slows down shrinking microtubules and has a second, though less potent, stabilizing effect at the microtubule end-structure. At the lattice Mal3 binds with low affinity and promotes microtubule rescues.

5.4 Additional remarks

Two recently published studies report the influence of EB1, the human end-binding protein, on microtubule dynamics *in vitro* [111,187]. Manna et. al [111] reports that EB1 had minimal effect on the microtubule growth speed and the rescue rate. The main effect was observed on the shrinkage speed and the catastrophe rate, the presence of EB1 decreasing disassembly speed and suppressing catastrophes. The only common observation between this study and our measurements with Mal3, is the observed decrease in the shrinkage speed. In the second report [187], Vitre et.al reveals yet an influence of EB1 on all dynamic instability parameters. The authors found that EB1 stimulates spontaneous nucleation and growth of microtubules, and promotes both catastrophes and rescues. The extent of the EB1 influence on microtubule dynamics is almost identical with our Mal3 measurements. Using cryo-electron-microscopy, the authors could observe longer tubulin sheets at the microtubule ends in the presence of EB1. Our similar observation corroborates with this result.

The differences between the two studies remain to be clarified. The experimental method used in [187] resembles closely our DIC method. Given the similarity between our observations, presented in this chapter, and the results from [187], one can conclude that the two homologs, EB1 and Mal3, rely on the same molecular mechanism to interact with microtubules and to influence microtubule dynamics.

Vitre et. al [187] propose a mechanism for catastrophes and growth enhancement based on EB1-stimulated growth and closure of the tubulin sheets: EB1 favors lateral association of free tubulin at microtubule-sheet edges. Based on our observations on the dynamic microtubule ends at high-resolution, we propose a mechanism in which Mal3 promotes formation of end-structures that frequently depolymerize, before having the chance to close into a tube. This mechanism might contribute to the observed enhancement of the catastrophe rate. Further experimental work is needed to clarify the molecular mechanism underlying the influence of Mal3 at microtubule ends.

5.5 Experimental procedures and data analysis

5.5.1 Measuring the parameters of microtubule dynamic instability by DIC microscopy.

Sample preparation. Experiments were performed in a flow chamber constructed between a microscope slide and a glass coverslip. Both glass surfaces were cleaned by immersion in chromosulfuric acid for few hours and subsequently rinsed with mili-Q water. The glass surfaces were separated by two parallel lines of silicone grease (high-vacuum silicone grease, Sigma) that were applied with a syringe on the microscope slide approximately 5 mm apart. The chamber was then filled with 6 μl of assay buffer (80 mM K-PIPES, 1 mM EGTA, 4 mM $MgCl_2$, pH 6.8) and the volume was adjusted by pressing the coverslip down until the liquid completely filled the chamber. Subsequent solutions were flowed in by pipetting on one side of the chamber and blotting with tissue or filter paper at the other side.

We used centrosomes (a kind gift from Bornens lab, Curie Institute; isolated from cultured human lymphoblastic cells [188]) as microtubule nucleation sites. First, the centrosomes were non-specifically adhered on the glass coverslip. The glass surface was then passivated in two steps by incubation with 0.2 mg/ml PLL-PEG (poly-L-lysine (20 kDa) grafted to polyethylenglycol (2 kDa) with 3.5 lysine units per PEG chain) (Susos AG, Switzerland) in assay buffer, and further with 1 mg/ml κ-casein in assay buffer. After each step, except the last incubation with κ-casein, the flow chamber was washed with 30-100 μl assay buffer. Passivation is necessary in order to minimize protein loss on the glass surfaces. Microtubule growth was initiated by flowing in a solution containing 15 μM tubulin (bovine, Cytoskeleton, USA), 1 mM GTP and Mal3 (with a concentration ranging from 20 nM to 2.5 μM) in assay buffer supplemented with 50 mM KCl, 0.1% methyl cellulose (4000cP, Sigma), 0.6 mg/ml κ-casein and an oxygen scavenger system (50 mM glucose, 400 μg/ml glucose-oxidase, 200 μg/ml catalase, 4 mM DTT). Methyl cellulose acts as a crowding agent preventing the microtubules to fluctuate away from the surface. Mal3 was a kind gift from Linda Sandblad (Brunner lab, EMBL) [25]. Before injection in the flow chamber, the tubulin solution was spun for 6 minutes in an airfuge (Beckman Coulter, A-100/30 rotor) at maximum speed (167000 x g) in order to remove protein aggregates from solution. The spinning was done with a cooled rotor in order to keep the tubulin solution below 10°C. After the tubulin solution was injected, the flow chamber was sealed with candle wax and transferred onto the microscope stage. Sample preparation was done at room temperature, 21°C. During the experiment, the temperature in the flow chamber was maintained at 25±1°C.

DIC microscopy. Dynamic microtubules nucleated from the centrosomes were imaged by video-enhanced differential interference contrast (VE-DIC) microscopy (figure 5.1 a, left), using an inverted microscope (DMIRB, Leica) equipped with a 100x/1.3 NA oil immersion objective (HCX PL FLUOTAR, Leica). The temperature in the sam-

ple was adjusted and maintained constant by Peltier elements (Melcor) mounted on a sleeve around the objective and controlled by in-house built electronics. Images were acquired with a CCD camera (CF8/1, Kappa), further processed for background substraction and contrast enhancement with an image processor (C5510 Argus 20, Hamamatsu Photonics) and digitized on-line at a rate of 1 frame per second (fps) with an in-house developed software (written and run in IDL). Simultaneously with the on-line digitization, the processed images were recorded on a DVD at video rate, 25 fps, with a commercial burner (DVD R-80, Philips).

After mounting on the microscope stage, the sample was first equilibrated to the set temperature, 25^{o}C, for about 10 minutes. Each sample was then imaged for 30-45 minutes.

Data analysis. Microtubule length vs time traces were measured using ImageJ software. Microtubule length changes below five pixels could not be observed, resulting in a spatial resolution of our assay of ~0.5 μm. Growing and shrinking speeds were determined from linear fits on individual events. One event is defined as a continuous growth or shrinking phase of a dynamic microtubule. For each sample an average growth and shrinkage speed was determined as the average over all events weighted with the time of the individual events (equation 5.1). The weighted standard deviation was determined as well (equation 5.2).

$$\mathrm{v}_s = \frac{\sum v_i t_i}{\sum t_i} \tag{5.1}$$

$$\mathrm{sd}_s = \sqrt{\frac{n}{n-1}\frac{\sum (v_i - \mathrm{v}_s)^2 t_i}{\sum t_i}} \tag{5.2}$$

where i denotes an individual event, v_i is the speed (growth or shrinkage) of the event i, t_i is the time spanned by the event i, and n is the total number of events measured in the sample.

For each Mal3 concentration, 30 - 75 microtubules were analyzed from 3 - 6 independent experiments. A weighted average speed (growth and shrinkage), v_s, was determined in each of these experiments. The speeds v_s (3 - 6 per Mal3 concentration) were further used to calculate an average speed, $\overline{\mathrm{v}}$, per Mal3 concentration. Figure 5.1 b, c shows ($\overline{\mathrm{v}} \pm \mathrm{sd}$). The standard deviation, sd, reflects the precision between different experiments at the same Mal3 concentration. We do not show the standard deviation, sd_s, on the average speed, v_s, within one experiment, which mostly reflects the intrinsic variability of the microtubule growth and shrinkage processes (see also text in section 5.2, page 85).

The catastrophe and rescue rates were determined by dividing the total number of catastrophes or rescues observed, N, by the total time the microtubules spent in the growing phase or, respectively, in the shrinking phase. For each Mal3 concentration

data was cumulated from the independent experiments. As both catastrophes and rescues are random events, the statistical error with which N was measured could be approximated by $\sqrt{N}$ (68.3% confidence level, corresponding to the standard deviation). This approximation only holds for large N (> 8). For Mal3 concentrations below 500 nM, we observed very few rescues (≤ 8). In this case only an upper bound (90% confidence level) could be estimated in determining N [53]. Another experimental consideration in measuring N is the limited spatial (~0.5 μm) and temporal (1 s) resolution of our assay. Missing the short and/or the fast events results in the underestimation of the catastrophe and the rescue rate, as well as apparent slower growth and shrinkage speeds. This effect could be important at high Mal3 concentrations (> 1 μM).

Control experiments. In our assay we used centrosomes as the microtubule nucleation sites. To check that our measurements on the dynamic instability parameters were not influenced by the possible residual proteins from the centrosome preparation, we prepared control samples in which microtubules were nucleated from seeds (short, stable GMPCPP microtubules) bound specifically on the surface of the flow chamber. The seeds were prepared by incubation of 30 μM tubulin mix containing 17% biotin-labelled tubulin with 1 mM GMPCPP (Jena Bioscience, Germany) at 36°C for 40 minutes. We used the same tubulin batch to prepare seeds and in the polymerization mix. The seeds were bound to a biotin-functionalized surface via biotin-straptavidin links. The surface was prepared by subsequent incubations with 0.2 mg/ml PLL-PEG-biotin (poly-L-lysine (20 KDa) grafted to polyethylenglycol (2 KDa) with 3.5 lysine units per PEG chain and with 48% biotin attached to PEG (3.4 KDa)(Susos AG, Switzerland) and with 1 mg/ml streptavidin in assay buffer.

We compared the dynamic instability parameters of microtubule plus-ends grown from centrosomes and from the seeds for five different experimental conditions: tubulin alone and in the presence of 50 - 500 nM Mal3. We measured similar microtubule dynamics in the samples with centrosomes and with seeds.

5.5.2 Evaluating the amount of Mal3 bound on microtubules by confocal microscopy

Sample preparation. The samples were prepared in a similar way as for the DIC experiments, with the exception that Mal3-Alexa 488 was used in the protein mix. The Mal3 protein was purified and labelled as described previously [19, 124] (see also chapter 4). The labelling ratio was 0.9 of Alexa 488 dye per Mal3 protein molecule. Experiments were performed at 15 μM tubulin.

Confocal microscopy. The fluorescently labelled Mal3 on dynamic microtubules was imaged with a confocal spinning disc microscope, comprising a confocal scanner unit (CSU22, Yokogawa Electric Corp) attached to an inverted microscope (DMIRB, Leica) equipped with a 100x/1.3 NA oil immersion lens (PL FLUOTAR, Leica) and a built-in

1.5x magnification lens. The sample was illuminated using a 488 nm laser (Sapphire 488-30 CHRH, Coherent Inc.). Images were captured by a cooled EM-CCD camera (C9100, Hamamatsu Photonics) controlled by software from VisiTech International. Images were acquired with exposures between 500 ms and 1 s. The laser intensity was varied depending on the Mal3 concentration in order to achieve a good signal to noise ratio. The temperature was controlled by maintaining the room at 25±1°C.

Image processing and profile analysis. We analyzed intensity profiles along growing microtubules. As we used different illumination conditions (laser intensity, exposure time and camera gain) for different samples, the raw images were first processed in order to be able to compare the microtubule profiles measured in different samples. Through the image processing we also corrected for the spatial illumination profile of our set-up, that had a 2D-Gaussian shape.

The intensity measured in each pixel of the raw image, $\mathrm{IM_{raw}}$, was the summed contribution of several signals:

$$\mathrm{IM_{raw}}(x,y) = \mathrm{N}(x,y)\cdot E(x,y)\cdot f(I_{\mathrm{laser}},g,t_{\mathrm{exp}}) + \mathrm{IM_0}(x,y) \tag{5.3}$$

$$\mathrm{IM_0}(x,y) = \mathrm{c_0}\cdot E(x,y)\cdot f(I_{\mathrm{laser}},g,t_{\mathrm{exp}}) + f_0(g,t_{\mathrm{exp}}) \tag{5.4}$$

where (x,y) is the pixel position, N is the number of Mal3-Alexa 488 molecules contributing to the signal of the pixel (x,y), E is the 2D-Gaussian profile of the illumination, f is a term that includes the non-linear dependency of the signal on the laser intensity, I_{laser}, and on the camera gain, g, and the linear dependency on the exposure time, t_{exp}. $\mathrm{IM_0}$ is the image acquired when there are no fluorescent molecules in the sample and it comprises two main contributions. One that depends on the laser intensity and was mainly due to laser leakage through the filters, and partly due to the autofluorescence of the glass and of the protein solution. This contribution can be written as the equivalent signal from a number $\mathrm{c_0}$ of fluorescent molecules ($\mathrm{c_0}$ should not depend on pixel position unless there are inhomogeneities on the filters or on the camera chip). The other contribution in $\mathrm{IM_0}$ was the dark camera noise f_0 (camera signal when the sample was not illuminated). We processed the raw image $\mathrm{IM_{raw}}$ as indicated in equation 5.5 and obtained a normalized intensity, I_{n}, that does not depend anymore on the illumination conditions.

$$\mathrm{IM_p}(x,y) = \frac{\mathrm{IM_{raw}}(x,y)-\mathrm{IM_0}(x,y)}{\mathrm{IM_{ctrl}}(x,y)-\mathrm{IM_0}(x,y)} \equiv I_{\mathrm{n}}(x,y) \propto \frac{\mathrm{N}(x,y)}{\mathrm{N_{ctrl}}(x,y)} \tag{5.5}$$

where $\mathrm{IM_{ctrl}}$ is an image acquired in a control sample containing a solution of 300 nM Mal3-Alexa 488 together with all the other components of the polymerization mix and no centrosomes on the surface, thus no growing microtubules. $\mathrm{N_{ctrl}}$ represents the number of fluorescent Mal3 molecules contributing to the signal in the control sample. These molecules were mainly diffusing and only a very small fraction were non-specifically adhered on the surface. In the raw image, along a microtubule, the main

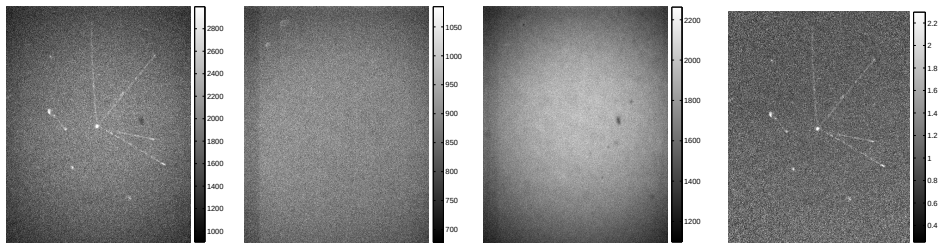

Figure 5.8: Image processing. From left to right: IM_{raw}, IM_0, IM_{ctrl}, and IM_p. The raw image was acquired in a sample with 300 nM Mal3-Alexa 488 and dynamic microtubules.

fraction of N was represented by the Mal3-Alexa 488 molecules interacting with the lattice or with the tip of the microtubule. Due to the different localizations within the point spread function of the microscope of the molecules (diffusing in solution or on surface) included in N and N_{ctrl}, the normalized intensity I_n, which we evaluated in the processed image IM_p, it is not equal, but proportional to the ratio N/N_{ctrl}. As N_{ctrl} was constant, any change in I_n along a microtubule or between samples directly reflects and it is proportional to real changes in N. The images IM_0, IM_{ctrl}, and IM_{raw} were taken at identical illumination conditions and at similar depth in the sample, i.e. close to the surface where the dynamic microtubules were localized. For IM_0 and IM_{ctrl} ten images were average to decrease imaging noise. An example of a processed image is shown in figure 5.8.

For almost half of the illumination conditions the signal measured in the control sample was low resulting in a very noisy difference image, $IM_{ctrl} - IM_0$, with the average intensity approximatively zero. In these cases we computed $I_n(x,y)$ using a control image acquired at different illumination conditions, IM'_{ctrl}, that had a better signal to noise ratio (equations 5.6 and 5.7).

$$IM'_p(x,y) = \frac{IM_{raw}(x,y) - IM_0(x,y)}{IM'_{ctrl}(x,y) - IM'_0(x,y)} \equiv I'_n(x,y) \tag{5.6}$$

$$I_n(x,y) = I'_n(x,y) \cdot \frac{b}{b'} \tag{5.7}$$

where b is the background intensity evaluated in IM_p (equation 5.5) by averaging the pixel intensities in a couple of rectangles that included only surface without microtubules. b' was evaluated in a similar way in the processed image IM'_p, which was calculated using the control image acquired at the different illumination condition. We did not detect any bias in I_n between the two ways of evaluating it.

In the processed images, intensity line profiles were measured on individual microtubules (figure 5.9). One microtubule profile was the average of three adjacent line

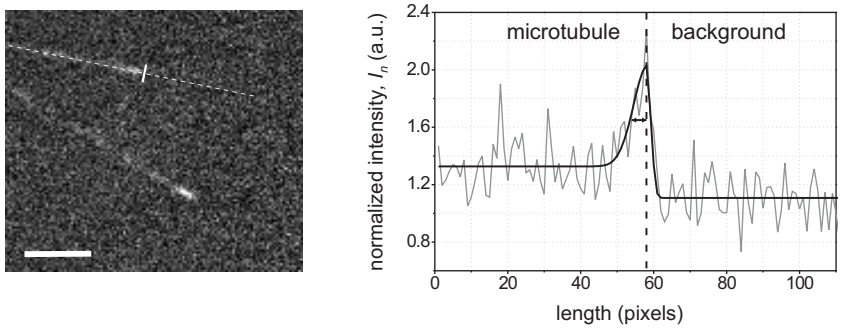

Figure 5.9: Microtubule line profile. Left: Fluorescent image of Mal3-Alexa 488 (500 nM) on dynamic microtubules. The line used to measure the profile (dotted line) was manually drawn and the initial guess of the microtubule tip (thick line) was evaluated from a step fit. Scale bar is 3 μm. Right: The profile measured in the left image is shown and superimposed is the result of a fit combing two half-Gaussians. The fit yielded the microtubule tip position ($x_{\text{tip}} = 58$) indicated by the dotted line and the standard deviation of the microtubule half-Gaussian ($\sigma_{\text{tip}} = 4 \pm 1$ pixels) indicated by the double arrowed line.

scans to account for the point spread function (PSF) of the microscope. The intensities along a line scan were binned to pixel-size bins (the length of one pixel corresponded to 110 nm). A profile typically included 1 - 5 μm stretch of the microtubule continuing with a 1 - 5 μm stretch on the surface, along the microtubule line. An initial guess of the tip location was evaluated from a step fit on the profile. This value was used as initial parameter for a fit with the functional form given by two half-Gaussians, one for the microtubule stretch and one for the background stretch (equations 5.8 and 5.9).

$$G_{\text{mt}} = I_{\text{background}} + I_{\text{lattice}} + I_0 e^{\frac{(x-x_{\text{tip}})^2}{2\sigma_{\text{tip}}^2}} \tag{5.8}$$

$$G_{\text{bkg}} = I_{\text{background}} + I_0 e^{\frac{(x-x_{\text{tip}})^2}{2\sigma_{\text{psf}}^2}} \tag{5.9}$$

The fit had three parameters: the microtubule tip location, x_{tip}, the standard deviation of the microtubule half-Gaussian, σ_{tip}, and the shared maximum value of the Gaussians, I_0. The standard deviation, σ_{psf}, of the half-Gaussian for the background part, G_{bkg}, was fixed to one pixel, corresponding to the PSF of our confocal microscope. The signal along the microtubule end region is also convolved with the PSF. Therefore, the standard deviation determined at the microtubule tip, σ_{tip}, includes also the σ_{psf}.

From the fit parameters we used the microtubule tip location, x_{tip}, to align the microtubule profiles in one sample and we next averaged the aligned profiles (figure 5.2 a). In each sample 10 - 70 microtubules were analyzed. The standard deviation of the mi-

crotubule half-Gaussian, σ_{tip}, was evaluated from the fit on each individual profile. This value indicates the average spatial extent of the Mal3 interacting with the microtubule tip.

The average background, $I_{background}$, was evaluated as the average pixel intensity in a rectangle on a surface area close to the microtubule, or as the average pixel intensity of the surface stretch of the profile starting three pixels away from the microtubule tip. The amount per pixel of Mal3 interacting with the lattice, given as the normalized intensity $I_{lattice}$, was evaluated in each sample from the average profile as the average pixel intensity more than $2\sigma_{tip}$ away from the microtubule tip minus $I_{background}$. The amount per pixel of Mal3 bound at the tip, I_{tip}, was evaluated as the average intensity of the pixels within the spatial extent σ_{tip} from the microtubule tip, minus $I_{background}$. The mean values and the corresponding s.e.m. for $I_{background}$, $I_{lattice}$, I_{tip}, and σ_{tip} (figure 5.2 b-e) were calculated averaging all the values estimated from fits on individual profiles in one sample.

Control experiments. We checked whether the Alexa 488 labelled Mal3, used for the confocal imaging, had the same behavior on microtubule dynamics as the unlabelled Mal3, used in the DIC experiment. We measured the dynamic instability parameters of microtubules grown in the presence of 100 nM and 200 nM Mal3-Alexa 488 and we found similar values with the ones evaluated for unlabelled Mal3. This agreement indicated that the presence of the Alexa label on Mal3 did not affect the protein interaction with the microtubules.

We also checked whether the binding of Mal3-Alexa 488 on microtubules was possibly influenced by residual proteins from the centrosome preparation. For this purpose we measured profiles on microtubules growing from the plus-ends of seeds (short stable GMPCPP microtubules). We did not find a difference in the amount of Mal3 present at the growing tip or on the microtubule lattice between the samples prepared with different nucleation sites.

5.5.3 Microtubule end dynamics measured with optical tweezers

Microtubules were nucleated from an axoneme. Growth and shrinkage of dynamic microtubules were monitored with high resolution using an optical tweezers based technique (method described in chapter 2).

Sample preparation. Microtubules grew against rigid barriers that were made from SU-8 photoresist (MicroChem) using standard lithography techniques [144, 150]. The coverslip carrying the SU-8 barriers were assembled into a home-made flow chamber. The chamber allowed injection of small samples (couple of microliters) by pipetting at an entrance opening and continuous slow flow by adjusting the hight of the drain. The drain and the chamber were connected by teflon tubing and a computer-linked flow sensor (Seyonic, Switzerland) was inserted between the drain and the chamber in or-

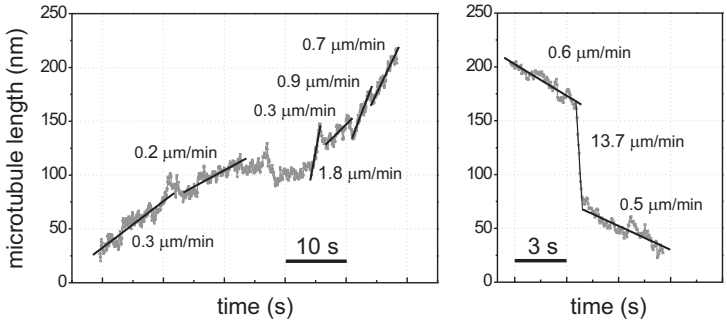

Figure 5.10: Evaluating growth and shrinkage speeds. Microtubule growth event (left) and the shrinkage event of the same microtubule (right). Solid black lines are linear fits on data stretched that have approximatively constant speed. The speed values resulted from the fits are indicated.

der to monitor the magnitude of the flow. Prior to the sample injection, the chamber was passivated with 50 mg/ml BSA. Streptavidin coated polystyrene beads (2 μm in diameter) were flowed in the chamber together with axoneme pieces (a kind gift from M. Footer). Using the optical trap a construct was assembled by non-specific attachment of a bead to one end of an axoneme. The construct was then positioned and held in front of a barrier by a 'key-hole' optical trap. Microtubule growth was initiated by flowing in the polymerization mix prepared in a similar way as for the DIC experiments.

Data acquisition and analysis. Microtubule growth against the rigid barrier resulted in bead displacement, which was measured off-line at a sampling rate of 25 Hz with the use of a standard auto-correlation method (in-house developed image processing software written and run in IDL). From the bead displacement we can evaluate the force against the growing microtubule (bead displacement multiplied with the trap stiffness) and the microtubule length after correction for the construct compliance. The construct compliance was determined before each experiment. With this method the microtubule length changes in time were processed with few nanometer resolution. Single events of growth and shrinkage were broken into a series of shorter events, stretches that could be approximated as having constant speed (figure 5.10). The growth and shrinkage speeds were evaluated from linear fits on these short data intervals and the corresponding weighted distributions were constructed. Each speed contribution was weighted with the time extent of the corresponding event (for the growth events) and with the total length change during the corresponding event (for the shrinkage events).

Acknowledgements

I would like to thank Linda Sandblad for the kind gift of Mal3 protein and useful discussions, Peter Bieling and Liedewij Laan for help with purification and labelling of

Mal3, Liedewij Laan for help with initial experiments, and Christian Tischer for useful discussions.

to be submitted: Munteanu EL, Laan L, Brunner D, Surrey T, Dogterom M. Regulation of microtubule dynamics, *in vitro*, by the autonomous microtubule-end tracker Mal3.